

## MIT Open Access Articles

*Electrochemical Determination of the Thermodynamic Properties of Lithium-Antimony Alloys*

The MIT Faculty has made this article openly available. **Please share** how this access benefits you. Your story matters.

**Citation:** Kane, M. M., J. M. Newhouse, and D. R. Sadoway. "Electrochemical Determination of the Thermodynamic Properties of Lithium-Antimony Alloys." *Journal of the Electrochemical Society* 162, no. 3 (December 31, 2014): A421–A425.

**As Published:** <http://dx.doi.org/10.1149/2.0671503jes>

**Publisher:** Electrochemical Society

**Persistent URL:** <http://hdl.handle.net/1721.1/102197>

**Version:** Final published version: final published article, as it appeared in a journal, conference proceedings, or other formally published context

**Terms of use:** Creative Commons Attribution





# Electrochemical Determination of the Thermodynamic Properties of Lithium-Antimony Alloys

Margaret M. Kane, Jocelyn M. Newhouse, and Donald R. Sadoway<sup>z</sup>

Department of Materials Science and Engineering, Massachusetts Institute of Technology, Cambridge, Massachusetts 02139-4307, USA

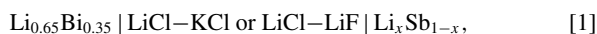
The variation in the high temperature thermodynamic properties of the Li-Sb system with temperature (425–775°C) and composition ( $x_{\text{Li}} = 0.01\text{--}0.75$ ) was determined by electromotive force (emf) measurements in a cell configured as follows: Li-Bi reference electrode ( $x_{\text{Bi}} = 0.35$ ) | eutectic of LiCl-KCl or LiCl-LiF | Li-Sb alloy. On the basis of these data the Li-Sb couple was deemed attractive for storage of electrical energy in a liquid metal battery. In addition, an updated Li-Sb binary phase diagram is proposed. © The Author(s) 2014. Published by ECS. This is an open access article distributed under the terms of the Creative Commons Attribution 4.0 License (CC BY, <http://creativecommons.org/licenses/by/4.0/>), which permits unrestricted reuse of the work in any medium, provided the original work is properly cited. [DOI: 10.1149/2.0671503jes] All rights reserved.

Manuscript submitted August 11, 2014; revised manuscript received December 19, 2014. Published December 31, 2014.

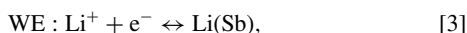
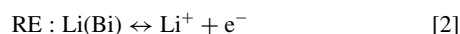
The lithium-antimony (Li-Sb) binary system is of interest for energy storage applications, specifically at high temperatures for liquid metal batteries, because of the mutual reactivity of these elements, their relative abundance in the earth's crust, and their comparatively low cost.<sup>1,2</sup> Prior investigations of this system are limited and are generally focused on intermetallic characterization.<sup>3–5</sup> Notably, two groups have studied the intermetallics  $\text{Li}_2\text{Sb(s)}$  and  $\text{Li}_3\text{Sb(s)}$  electrochemically, determining the thermodynamic electric potential and Gibbs free energy of formation of the compounds between 355°C and 600°C.<sup>3,6,7</sup> As for liquid alloys, Nikitin et al.<sup>3</sup> studied the deposition of lithium by cathodic polarization of liquid antimony and observed that electrode potential varied inversely with both current density and degree of lithiation, which they attributed to formation of composition gradients.

In 1993 Sangster and Dalton presented a calculated Li-Sb phase diagram,<sup>4</sup> however, for liquid interactions they relied on data from the Li-Bi system due to a perceived lack of thermodynamic data for Li-Sb liquid alloys. Two years later Fedorov<sup>8</sup> published an alternate version of the Li-Sb phase diagram determined from cooling curves (cooling rate unknown), specifying that it was a non-equilibrium phase diagram, an opinion expressed by others.<sup>9</sup>

In the present study electromotive force (emf) measurements characterize the thermodynamic properties of Li in Li-Sb liquid alloys between 425°C and 775°C. Emf measurements have been used to accurately characterize similar lithium binary systems in the past.<sup>10–14</sup> The Li-Sb system was studied in this work using the electrochemical cell



where a Li-Bi two phase alloy served as the reference electrode (RE), the Li-Sb alloys of various concentrations served as the working electrode (WE), and either of the two eutectic binary molten salts as the electrolyte. The half cell reactions of this cell are



and the full cell reaction is



where the parentheses indicate the solvent metal. The open circuit potential (OCP) at equilibrium  $E_{\text{cell}}$  is related to the Gibbs free energy of reaction  $\Delta_r G$  via the Nernst equation

$$\Delta_r G = -nFE_{\text{cell}} = -RT \ln \left( \frac{a_{\text{Li(Sb)}}}{a_{\text{Li(Bi)}}} \right), \quad [5]$$

where  $n$  is the number of electrons transferred (in this system,  $n = 1$ ) and  $a_{\text{Li}}$  is the activity of Li with respect to the standard state.

<sup>z</sup>E-mail: dsadoway@mit.edu

When OCP is measured as a function of temperature, slope changes indicate phase changes, thereby allowing for confirmation<sup>15,16</sup> or refinement<sup>17,18</sup> of the binary phase diagram.

## Methods

**Electrode preparation.**— For the working electrodes ( $\sim 0.3 \text{ cm}^3$  volume), Sb (99.999% Alfa Aesar) and Li (99.9% Sigma Aldrich) were combined in pyrolytic boron nitride crucibles ( $\sim 2.0 \text{ cm}$  height,  $\sim 1.2 \text{ cm}$  diameter). The metal masses depended on the desired alloy composition. Alloying was achieved by induction melting of the Sb, followed by incremental addition of Li. After Li inclusion, the liquid metal mixture was stirred with a tungsten wire lead (99.95% Alfa Aesar) before cooling (Figure 1a). For the reference electrodes, a combination of 35 at% Bi (99.999% Sigma Aldrich) and 65 at% Li were similarly induction melted until complete liquification was achieved. All preparation was done in a glove box under a purified argon atmosphere ( $\sim 0.1 \text{ ppm O}_2$ ).

**Vessel assembly.**— The electrodes were placed in an alumina crucible ( $\sim 10 \text{ cm}$  height,  $\sim 5.5 \text{ cm}$  diameter) at the base of a stainless steel vessel (Figure 1b). The tungsten leads were sleeved in alumina tubing to electrically insulate them from the test vessel. The powdered electrolyte ( $\sim 113 \text{ cm}^3$ ) was then poured into the alumina crucible with the electrodes. Two electrolytes were used in the study: (1) a eutectic mixture of LiCl-KCl (59 at% LiCl, 49 at% KCl) and (2) a eutectic mixture of LiCl-LiF (70 at% LiCl, 30 at% LiF).

**OCP procedure.**— After removal from the glove box, the sealed vessel was placed in a vertical tube furnace and put under active vacuum ( $\sim 1 \text{ Pa}$ ) at 80°C for 10 h and 230°C for 8 h. The atmosphere of the vessel was then purged with ultra high purity Ar (Airgas, 6 ppm  $\text{O}_2$ ) three times to flush the system. Ar flowed slowly for the remainder of the experiment. The temperature was then increased to 630°C, at which point the OCP measurements were initiated. The temperature of the furnace was changed at a maximum rate of 5°C/minute, and the electrochemical cell was allowed to equilibrate for 60 minutes ( $\leq 10^\circ\text{C}$  steps) or 90 minutes (25–30°C steps) at each temperature. The internal temperature of the electrolyte was measured with an ASTM type-K thermocouple.

Potential measurements were taken sequentially between one of the reference electrodes and one of the working electrodes for 2 minutes each using a potentiostat/galvanostat (Autolab PGSTAT302N, Metrohm). In data processing, only temperature measurements with variation of less than 0.5°C for  $\pm 6$  minutes were considered.

**References electrodes.**— The Li-Bi reference electrodes were chosen for their superior stability compared to that of pure Li and to reduce the dissolution of Li into the salt.<sup>14</sup> The Li-Bi system has been extensively characterized and the thermodynamic electric potential of the

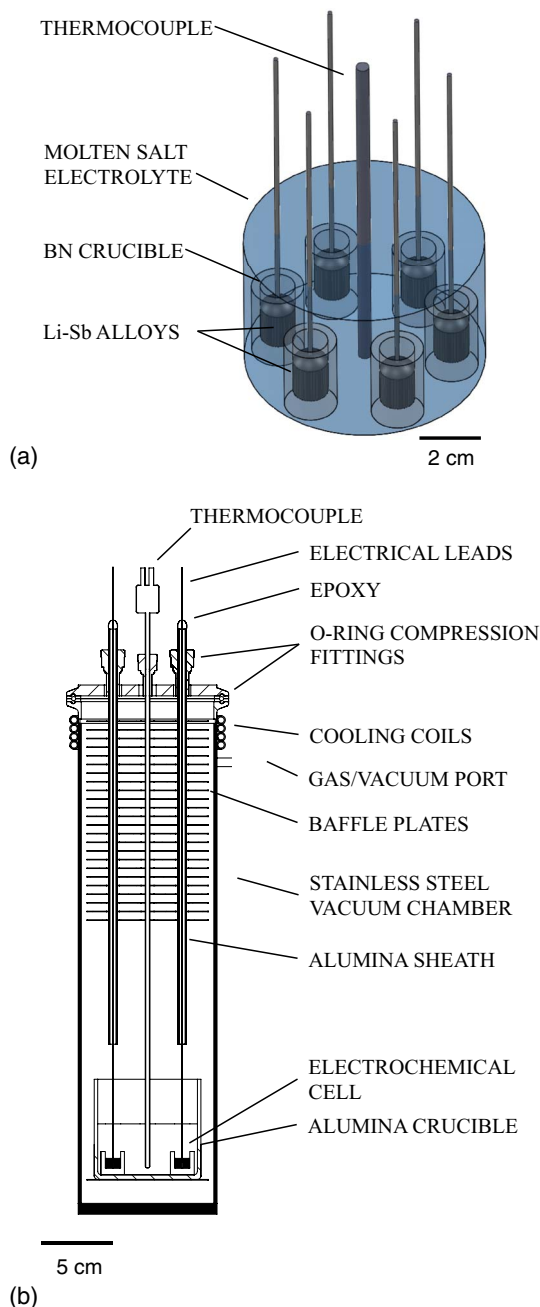


**Figure 1.** Schematic the open circuit potential measurements experimental setup: (a) electrochemical cell with molten KCl-LiCl or LiF-LiCl electrolyte (b) cross-section of the test vessel containing the electrochemical cell. Scale bar is approximate.

Li-Sb working electrodes with respect to pure Li,

$$E_{WE} = \frac{RT}{F} \ln \left( \frac{a_{Li(Sb)}}{a_{Li(l)}} \right) \quad [6]$$

is calculated by adding the reference electrode potential vs. the standard state  $E_{RE}$  to the recorded OCP

$$E_{WE} = E_{cell} + E_{RE}. \quad [7]$$

The conversion of the OCP data to a new reference system was achieved using the data of Gasior and Moser<sup>14</sup>

$$E_{RE} \text{ (mV)} = -1683.2 - 0.903T + 465.66 \ln T, \quad [8]$$

where  $T$  is the absolute temperature (K). Going forward, the notation will be simplified:  $E_{WE} \rightarrow E$ ,  $X_{Li(Sb)} \rightarrow X_{Li}$  where  $X$  is a generic thermodynamic variable, and emf will be used to indicate electric potential versus the standard state.

**Experimental error.**— The error in the calculated values arises from the dependence of the emf on composition and from calibration of the Li-Bi reference electrode. The uncertainty in concentration varies with composition but is generally less than 0.1 at% Li ( $\pm 0.1$  mg Li). Another source of error derives from calibration of the reference electrode, for which the reported error is  $\sim 10$  mV.<sup>14</sup> This uncertainty adds an additional 1–2% error to the converted  $E_{WE}$  values. The calibration is also dependent on the measured temperature, for which the uncertainty is approximately  $\pm 2^\circ\text{C}$  radially ( $\sim 0.5\%$ ).

## Results and Discussion

**Emf data.**— Using the electrochemical cell described in Equation 1, the OCP measurements for the Li-Sb working electrodes were taken at Li concentrations varying from  $x_{Li} = 0.01$  to 0.75 in contact with an electrolyte composed of a eutectic mixture of LiCl-KCl or LiCl-LiI. Heating and cooling sequences were performed at the same compositions with different electrolytes to probe the reproducibility of the results.

The compiled data from the various tests are presented in Figure 2. The emf values for a variety of Li-Sb alloys at different temperatures are shown referenced to Li(l) using Equations 7 and 8, with slope changes indicating changes of phases for a given composition. Data measured with increasing and decreasing steps reveal good agreement over the course of the experiment, although some compositions show hysteresis, specifically at  $x_{Li} = 0.01$  and 0.25. Significant undercooling can also be observed at low Li concentrations and will be discussed in the following section.

At the lowest temperatures the emf values exhibit two distinct solid-solid regions. All alloy compositions between  $0.01 \leq x_{Li} < 0.66$  converge to one line below  $460^\circ\text{C}$ , suggesting the two phases present are Sb(s) and  $\text{Li}_2\text{Sb}(s)$ . The second two-phase region is most likely  $\text{Li}_2\text{Sb}(s) + \text{Li}_3\text{Sb}(s)$  as the emf data for  $0.66 \leq x_{Li} < 0.75$  converge below  $580^\circ\text{C}$ . Of note is the divergent behavior of the  $x_{Li} = 0.75$  sample with increasing temperature (labeled  $\text{Li}_{3+\delta}\text{Sb}(s)$  in Figure 2). The data are consistent with a two-phase to single-phase transition,

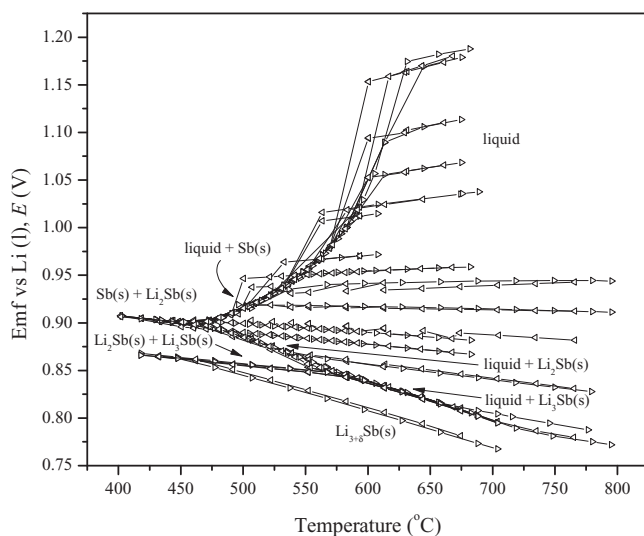


**Figure 2.** Variation of electromotive force with temperature and composition  $0.01 < x_{Li} < 0.75$  for Li(l)|LiCl-KCl or LiCl-LiI|Li-Sb cells. Data taken on both heating, ' $\triangleright$ ', and cooling, ' $\triangleleft$ ', are reported. Lines shown are connections between data points.

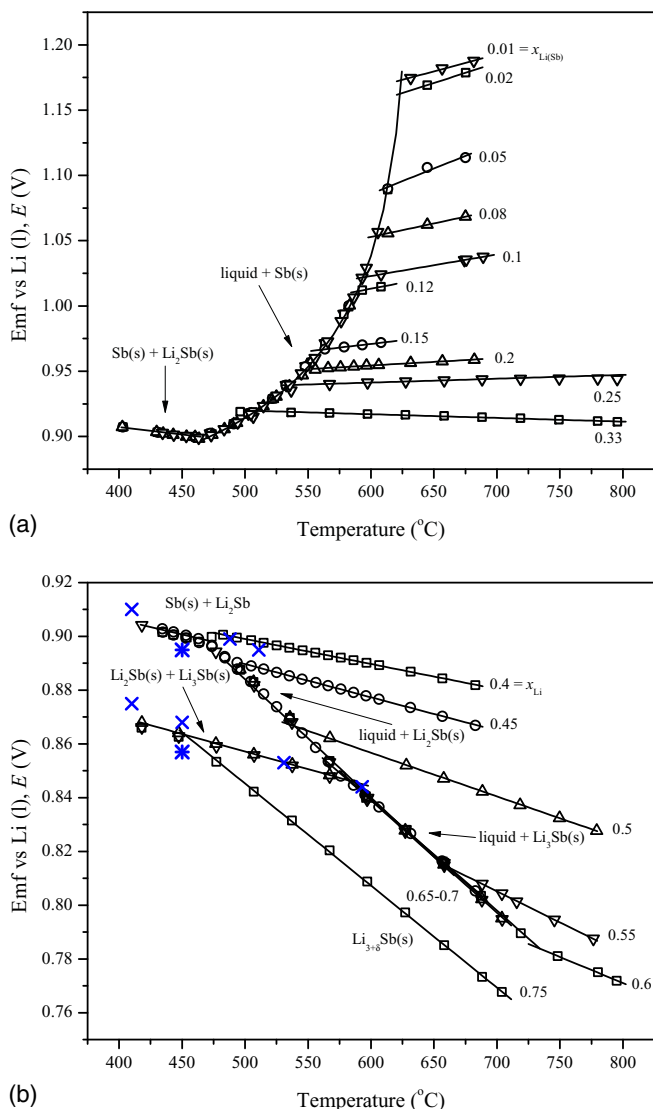


**Figure 3.** Variation of electromotive force with temperature for Li(l)|LiCl-KCl|Li-Sb cells for compositions (a)  $0.01 \leq x_{\text{Li}} \leq 0.33$  and (b)  $0.4 \leq x_{\text{Li}} \leq 0.75$ . Linear fits were used for data in single-phase and solid-solid regions. For liquid-solid two-phase regions non-linear fits were used (Eq. 10, 12). Select data from Figure 6 in Weppner and Huggins,<sup>4</sup> 'x', and Nikitin et al.,<sup>5</sup> '\*', are included for comparison.

suggesting that above 445°C the alloy enters a region of greater off-stoichiometric solubility of the intermetallic.

At the highest temperatures the emf values differentiate by composition along lines each representing single-phase alloys. At intermediate temperatures, three liquid + solid two-phase regions are observed: (1) for  $x_{\text{Li}} \leq 0.40$ , Sb(s) + liquid; (2) for  $0.40 < x_{\text{Li}} < 0.55$ ,  $\text{Li}_2\text{Sb(s)} + \text{liquid}$ ; and (3) for  $0.55 \leq x_{\text{Li}} < 0.75$  at  $T > 560^\circ\text{C}$ ,  $\text{Li}_3\text{Sb(s)} + \text{liquid}$ . Select Li-Sb two-phase emf data of Weppner and Huggins<sup>6</sup> and relaxation data of Nikitin et al.<sup>3</sup> are included in Figure 3b for comparison and match well with the current investigation ( $\pm 10$  mV).

**Undercooling.**— As can be seen in Figure 2, the low Li content Li-Sb alloys exhibit severe undercooling. The samples maintain their liquid state approximately 50°C (up to 4 hours) past the slope change noted with an increasing temperature regime. The extension of the linear behavior past the data collected on heating cycles is consistent with undercooling, which could account for the differences between the phase diagram constructed using cooling curve data<sup>8</sup> and the re-

**Table I.** Linear fits of emf  $E$  vs  $T$  data in single-phase regions,  $0.01 \leq x_{\text{Li}} \leq 0.75$  (Eq. 9). Valid temperature ranges are indicated. Error values represent 95% confidence bounds. The superscript 'a' denotes tests that were performed using a LiCl-KCl salt and the superscript 'b' denotes tests that were performed using a LiCl-LiF salt.

$x_{\text{Li}}$	$\frac{\Delta \bar{S}_{\text{Li}}}{F}$ ( $\times 10^5$ V K <sup>-1</sup> )	$\frac{-\Delta \bar{H}_{\text{Li}}}{F}$ ( $\times 10^2$ V)	R <sup>2</sup>	T range (K)
0.008 <sup>a</sup>	24 ± 5	95 ± 5	0.8501	875–950
0.02 <sup>a</sup>	31 ± 1	88 ± 1	0.9993	870–950
0.05 <sup>a</sup>	30 ± 18	80 ± 17	0.8336	915–950
0.08 <sup>a</sup>	21 ± 1	87 ± 1	0.9987	880–950
0.10 <sup>a</sup>	13.5 ± 0.3	88.5 ± 0.3	0.9995	885–950
0.12 <sup>a</sup>	17.3 ± 0.6	86.2 ± 0.5	0.9972	865–880
0.15 <sup>a</sup>	11.1 ± 0.2	87.4 ± 0.2	0.9981	830–885
0.20 <sup>b</sup>	9.4 ± 0.4	88.0 ± 0.3	0.9923	835–885
0.25 <sup>b</sup>	5.0 ± 0.2	90.0 ± 0.2	0.9867	820–880
0.33 <sup>b</sup>	-8.13 ± 0.05	96.6 ± 0.1	0.9996	780–1050
0.40 <sup>b</sup>	-9.32 ± 0.04	97 ± 1	0.9997	750–960
0.45 <sup>b</sup>	-12.36 ± 0.04	98.52 ± 0.04	0.9998	760–960
0.50 <sup>a</sup>	-16.1 ± 0.1	99.7 ± 0.1	0.997	840–1070
0.55 <sup>a</sup>	-23.22 ± 0.05	103.1	1.0	960–1070
0.61 <sup>b</sup>	-19.3 ± 0.8	97.8 ± 0.7	0.9963	990–1070
0.75 <sup>a</sup>	-39 ± 2	115 ± 2	0.9745	735–975

sults of this study. Due to this observed phenomenon, only values obtained during heating were used for data analysis.

**Data analysis.**— Above the liquidus, the emf data are observed to vary linearly with temperature, consistent with the combined Nernst and Gibbs-Helmholtz relation

$$E = \frac{-\Delta \bar{H}_{\text{Li}}}{F} + \frac{\Delta \bar{S}_{\text{Li}}}{F} T \quad [9]$$

where  $\Delta \bar{H}_{\text{Li}}$  and  $\Delta \bar{S}_{\text{Li}}$  are the partial molar enthalpy and entropy of Li in the Li-Sb alloy, respectively. Linear fits of the emf vs. temperature of the single-phase liquid regions are shown in Figure 3 and reported in Table I.

The lower Li concentrations show evidence of a liquid-solid two-phase region above 460°C. The data can be fit using the procedure outlined in<sup>16</sup> given the following equation

$$E = A - BT \ln(T_m - T) + CT, \quad [10]$$

where  $T_m$  is the melting temperature of the solvent metal, in this case Sb. The emf data of  $x_{\text{Li}} = 0.01$  to 0.33 between 400–795°C were fit using Equation 10 and the resulting curve is shown in Figure 3a. The solubility of the Sb-rich solid solution  $x_{\text{Li(ss-Sb)}}$  can be calculated from this fit according to the previous derivation<sup>16</sup>

$$x_{\text{Li(ss-Sb)}} = (T_m - T_e) \exp \left\{ C \frac{nF}{R} \right\} \quad [11]$$

where  $T_e$  is the low Li side eutectic temperature (460°C). The current data give  $x_{\text{Li(ss-Sb)}} = 0.002$ , which is consistent with the behavior of the  $x_{\text{Li}} = 0.01$  alloy.

For the  $\text{Li}_2\text{Sb(s)} + \text{liquid}$  and  $\text{Li}_3\text{Sb(s)} + \text{liquid}$  two-phase regions, a more generic equation was used to fit the data<sup>19,20</sup>

$$E = A - BT \ln(T) + CT. \quad [12]$$

The curves resulting from these fits are shown in Figure 3b and match the data well. The coefficients for the non-linear fits to these two-phase regions can be found in Table II.

The fits to the data were used to calculate the emf values at 550°C, 600°C, and 650°C, which are plotted in Figure 4 and reported in Table III. The activity of Li can be related to emf by the following equation

$$a_{\text{Li}} = \exp \left\{ \frac{FE}{RT} \right\} \quad [13]$$

**Table II. Non-linear fits of temperature dependence of emf data in two-phase regions. The Sb(s) + liquid data were fit to Eq. 10,  $E = A - BT \ln(T_m - T) + CT$ .  $\text{Li}_2\text{Sb(s)} + \text{liquid}$  and  $\text{Li}_3\text{Sb(s)} + \text{liquid}$  data were fit to Eq. 12,  $E = A - BT \ln(T) + CT$ . Valid temperature ranges are listed. Error values represent 95% confidence bounds.**

2-Phase region	Eq.	A	B	C	$T_m$ (K)	$R^2$	T range (K)
Sb(s) + liquid	10	$0.91 \pm .02$	$9.8 \pm .2 \times 10^{-5}$	$-4.8 \pm .2 \times 10^{-4}$	904	0.9986	750–875
$\text{Li}_2\text{Sb(s)} + \text{liquid}$	12	$0.04 \pm .1$	$1.5 \pm .2 \times 10^{-3}$	$1.1 \pm .2 \times 10^{-2}$	–	0.9991	750–850
$\text{Li}_3\text{Sb(s)} + \text{liquid}$	12	$0.72 \pm .03$	$5.3 \pm .3 \times 10^{-4}$	$3.7 \pm .3 \times 10^{-3}$	–	0.9998	850–1050

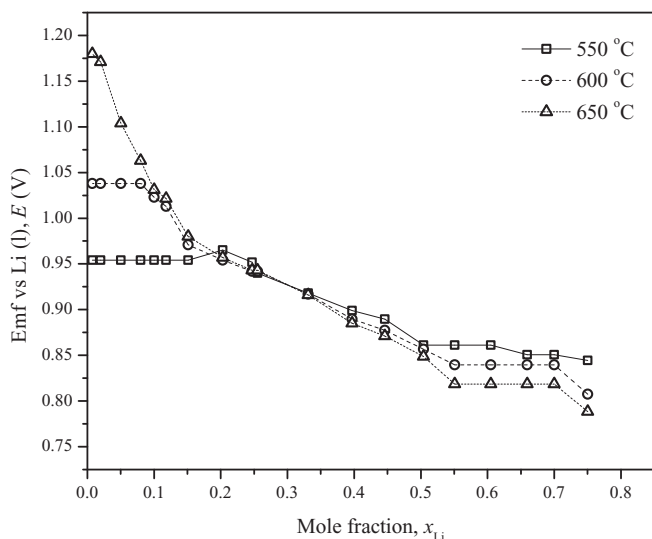


**Figure 4.** Electromotive force isotherms with increasing Li content at 550°C, 600°C, and 650°C.

When the alloy is all-liquid  $a_{\text{Li}}$  varies continuously with composition, as corresponds to the sloping regions in the emf vs. composition data. In contrast, when the alloy is present as two phases  $a_{\text{Li}}$  is independent of bulk concentration, as indicated by plateaus in the data. The isothermal curves cross at  $x_{\text{Li}} \approx 0.33$ , which is consistent with the sign change of the partial molar entropy of Li (see Table I).

**Table III. Measured emf  $E$  and calculated activity of liquid lithium  $a_{\text{Li}}$  (Eq. 13) at 550°C, 600°C, and 650°C.**

$x_{\text{Li}}$	550°C		600°C		650°C	
	$E$ (V)	$a_{\text{Li}} \times 10^5$	$E$ (V)	$a_{\text{Li}} \times 10^5$	$E$ (V)	$a_{\text{Li}} \times 10^5$
0.008	0.954	6.95	1.04	11.0	1.18	27.8
0.02	0.954	6.95	1.04	11.0	1.17	24.5
0.05	0.954	6.95	1.04	11.0	1.10	10.2
0.08	0.954	6.95	1.04	11.0	1.06	6.14
0.10	0.954	6.95	1.04	11.0	1.03	4.21
0.12	0.954	6.95	1.01	6.78	1.02	3.71
0.15	0.954	6.95	0.971	4.03	0.980	2.25
0.20	0.965	8.12	0.954	3.22	0.957	1.68
0.25	0.952	6.76	0.942	2.74	0.943	1.41
0.33	0.918	4.19	0.917	1.97	0.916	1.00
0.40	0.899	3.20	0.890	1.37	0.885	0.680
0.45	0.890	2.82	0.877	1.16	0.871	0.570
0.50	0.861	1.87	0.857	0.886	0.849	0.432
0.55	0.861	1.87	0.840	0.707	0.818	0.293
0.61	0.861	1.87	0.840	0.707	0.818	0.293
0.66	0.851	1.63	0.840	0.707	0.818	0.293
0.70	0.851	1.63	0.840	0.707	0.818	0.293
0.75	0.845	1.50	0.807	0.456	0.788	0.201

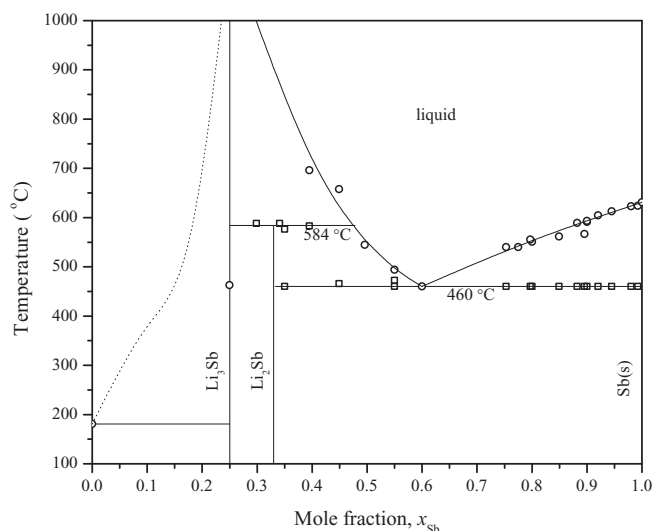


**Figure 5.** Suggested phase diagram for the Li-Sb binary system based on slope changes in emf vs. temperature data. Two-phase to single-phase, ‘○’, and two-phase to two-phase, ‘□’, transitions upon heating are indicated.

*Phase diagram.*— Based on the emf data reported above an alternative phase diagram for the Li-Sb binary system is proposed (Figure 5). The temperatures of phase transitions were determined from the intersections of curve fits of the data (Tables I and II). The two types of transition indicated in Figure 5, two-phase to single-phase or two-phase to two-phase, were distinguished by the compositional dependence of the slope change: the former occur at a single composition, while the latter occur at multiple compositions. The melting temperature of  $\text{Li}_3\text{Sb}$  was assumed to be above 1000°C<sup>8</sup> and the curvature of the liquid(Li rich) +  $\text{Li}_3\text{Sb(s)}$  liquidus line was adapted from Ref. 8 due to a lack of high Li concentration data in the present study.

Though other intermetallic compounds have been suggested in a previous phase diagram,<sup>8</sup> the emf data collected are consistent with the existence of only  $\text{Li}_2\text{Sb}$  and  $\text{Li}_3\text{Sb}$ , a conclusion supported by recent reviews of the Li-Sb binary system.<sup>5,21</sup> The low-Li eutectic temperature observed, 460°C, is slightly lower than those reported by Federov<sup>8</sup> and Nikitin et al.,<sup>3</sup> 466°C and 472°C, respectively; however, the eutectic composition of  $x_{\text{Li}} \approx 0.40$  observed in the present study is much higher than was presented in previous work.<sup>3,4,8</sup> Evidence of the peritectic reaction of  $\text{Li}_2\text{Sb(s)}$  decomposing into  $\text{Li}_3\text{Sb(s)}$  + liquid was observed at a much lower temperature than that postulated by Sangster, et al.<sup>4</sup> (580°C vs. 825°C). Structural analysis was outside the scope of this work.

## Conclusions

With a view to assessing the utility of the Li-Sb system in all-liquid electrochemical energy storage devices the thermodynamic properties of Li-Sb alloys were determined by emf measurements. In parallel, an alternative Li-Sb binary phase diagram has been proposed. The significant undercooling observed in this system may prove advantageous for extending the practical range of operation of liquid metal batteries.



### Acknowledgments

The financial support of TOTAL, S.A. and the John Reed UROP Fund at MIT is gratefully acknowledged. The authors thank Dr. Kangli Wang and Dr. Sophie Poizeau for leading us to this interesting system.

### References

- H. Kim, D. A. Boysen, J. M. Newhouse, B. L. Spatocco, B. Chung, P. J. Burke, D. J. Bradwell, K. Jiang, A. A. Tomaszowska, K. Wang, W. Wei, L. A. Ortiz, S. A. Barriga, S. M. Poizeau, and D. R. Sadoway, "Liquid Metal Batteries: Past, Present, and Future," *Chem. Rev.*, **113**(3), 2075 (2013).
- K. Wang, K. Jiang, B. Chung, T. Ouchi, P. J. Burke, D. A. Boysen, D. J. Bradwell, H. Kim, U. Muecke, and D. R. Sadoway, "Lithium-antimony-lead liquid metal battery for grid-level energy storage," *Nature*, **514**(7522), 348.
- A. V. Nikitin, A. I. Demidov, and A. G. Morachevskii, "Study of alloy formation in the cathodic polarization of antimony in molten salts," *Zh. Prikl. Khim. (Leningrad)*, **53**(7), 1641 (1980).
- J. Sangster and A. D. Pelton, "The Li-Sb (Lithium-Antimony) System," *J. Phase Equilib.*, **14**(4), 514 (1993).
- A. G. Morachevskii, "Thermodynamic Analysis of Alloys of the Lithium-Antimony System," *Russ. J. Appl. Chem.*, **75**(3), 367 (2002).
- W. Weppner and R. A. Huggins, "Thermodynamic Properties of the Intermetallic Systems Lithium-Antimony and Lithium-Bismuth," *J. Electrochem. Soc.*, **125**(1), 7 (1978).
- A. V. Nikitin, A. I. Demidov, A. G. Morachevskii, V. A. Matveev, and O. I. Ilina, "Thermodynamics of lithium-antimony system solid alloys," *Zh. Prikl. Khim. (Leningrad)*, **55**(4), 915 (1982).
- P. I. Fedorov, "Lithium-Antimony System," *Russ. J. Inorg. Chem.*, **40**(5), 815 (1995).
- C. Guminski and H. U. Borgstedt, "Regularities and peculiarities of the lithium binary phase diagrams," *Arch. Metall. Mater.*, **49**, 529 (2004).
- M. S. Foster, S. E. Wood, and C. E. Crouthamel, "Thermodynamics of Binary Alloys. I. The Lithium-Bismuth System," *Inorganic Chemistry*, **3**(10), 1428 (1964).
- R. A. Sharma and R. N. Seefurth, "Thermodynamic Properties of the Lithium-Silicon System," *Trans. Electrochem. Soc.*, **123**(12), 1763 (1976).
- M. L. Saboungi, J. Marr, and M. Blander, "Thermodynamic properties of a quasi-ionic alloy from electromotive force measurements: The Li-Pb system," *J. Chem. Phys.*, **68**, 1375 (1978).
- W. Sitte and W. Weppner, "Thermodynamics and phase stabilities of the ternary system Li-In-Sb," *Appl. Phys. A*, **38**(1), 31 (1985).
- W. Gasior and Z. Moser, "Thermodynamic study of liquid lithium-lead alloys using the emf method," *J. Nucl. Mater.*, **294**(1), 77 (2001).
- M. Notin and J. Hertz, "Thermodynamic data for calcium-based alloys from a new galvanic method," *Calphad*, **6**(1), 49 (1982).
- J. M. Newhouse, S. Poizeau, H. Kim, B. L. Spatocco, and D. R. Sadoway, "Thermodynamic properties of calcium-magnesium alloys determined by emf measurements," *Electrochim. Acta*, **91**, 293 (2013).
- S. Poizeau, H. Kim, J. M. Newhouse, B. L. Spatocco, and D. R. Sadoway, "Determination and modeling of the thermodynamic properties of liquid calcium-antimony alloys," *Electrochim. Acta*, **76**, 8 (2012).
- H. Kim, D. A. Boysen, D. J. Bradwell, B. Chung, K. Jiang, A. A. Tomaszowska, K. Wang, W. Wei, and D. R. Sadoway, "Thermodynamic properties of Ca-Bi alloys determined by emf measurements," *Electrochim. Acta*, **60**, 154 (2012).
- Y. Rao and B. Patil, "Thermodynamic study of the Mg-Sb system," *Metall and Materi Trans B*, **2**(7), 1829 (1971).
- A. Petric, A. D. Pelton, and M. L. Saboungi, "Thermodynamic properties of liquid K-Bi alloys by electromotive force measurements," *J. Phys. F: Met. Phys.*, **18**, 1473 (1988).
- M. E. Schlesinger, "Thermodynamic Properties of Solid Binary Antimonides," *Chem. Rev.*, **113**, 8066 (2013).